3

Preparation and Photoelectrochemical Properties of Fe_2O_3-TiO_2 based Photoanode for Water Splitting

Aryan Azad[1], Wooseung Kang[2] and Sun-Jae Kim[3]

[1]Institute/Faculty of Nanotechnology and Advanced Materials Engineering, Sejong University, Seoul 143-747, Korea
[2]Department of Environmental Engineering, Sunchon National University, Sunchon 540-74, Korea
[3]Institute/Faculty of Nanotechnology and Advanced Materials Engineering, Sejong University, Seoul 143-747, Korea

Outline:

Introduction

In this chapter, we reviewed nanostructured Fe_2O_3/TiO_2/FTO (fluorine-doped tin oxide) systems based on our published papers in terms of processing and photoelectrochemical (PEC) properties for water splitting. Due to environment pollution and limited supply issues of the conventional energy source of fossil fuels, alternative energy sources have been actively and extensively sought. One of the candidate energy sources is hydrogen, which can be generated through water splitting by utilizing of photoelectrochemical (PEC) process. The transformation of solar energy into chemical energy stored in the form of hydrogen is a promising method with the important advantages of being environment friendly and free from carbon dioxide emission. For the production of hydrogen through PEC water splitting process, transition metal oxide semiconductors have been considered to be promising materials. Among the transition metal oxide semiconductors, Fe_2O_3 has been one of the most extensively explored materials as a candidate electrode. Compared to other semiconductor materials, hematite (α-Fe_2O_3) has many potential advantages for hydrogen production in PEC devices [1, 2]. It is an n-type semiconductor that is stable in most electrolytes at pH > 3 and has a relatively narrow band gap of 2-2.2 eV, sufficient enough to utilize approximately 40% of the incident sunlight. Furthermore, it is abundant, inexpensive, and environmentally benign. Several factors, however, have limited the use of the hematite in photocatalytic hydrogen production applications including poor conductivity and high electron-hole pair recombination rates. In addition, the energy of the conduction band edge relative to the redox level of H^+/H_2 is thought to hinder charge transfers for the reduction reaction. Along with the Fe_2O_3 transition metal oxide semiconductor, TiO_2 has also been extensively investigated as an electrode material because of its favorable characteristics, such as high chemical stability, non-toxicity, and low fabrication cost, etc. Although TiO_2 has several advantages as described above, it has two critical limitations. The first is that exciton creation, the e-h+ precursor, is achieved only with UV light, rendering the use of solar irradiation inefficient because of the wide band gap of the most common polymorphic forms of TiO_2 (3.0 eV for rutile and 3.2 eV for anatase) [3]. Second, the large band-gap oxide semiconductors, such as n-type TiO_2 or WO_3 employed in photoelectrochemical devices, often have short exciton diffusion lengths, so it is mainly the carriers generated within the space charge layer that contribute to the photocurrent [4]. To maximize the water splitting efficiency of a TiO_2 photoanode, one would like (1) a narrower band gap to utilize visible-light energy, (2) a high contact area with the electrolyte to increase the splitting of the e-h+ pairs, and (3) a thicker film to increase the total absorption of solar light. As a way to improve the performance of PEC cells fabricated with Fe_2O_3 or TiO_2 material only, the approach of combining Fe_2O_3 and TiO_2 thin films to take advantages of the constituent materials has drawn much attention. Compared with pure TiO_2, the combined structure of Fe_2O_3 and TiO_2 thin film has higher specific surface area, low combination of electrons and holes, and red-shift in light absorption. [5-7]. Fe^{+3} ions reduced the value of the band gap energy of TiO_2, making the modified samples able to absorb light in the visible region. Under the radiation of LED lighting the ability to degrade p-xylene of the modified Fe-TiO_2 samples has been found to be 2-3 times higher than that of pure TiO_2 [8]. As a way of improving the performance of the Fe_2O_3-based photoanode for a photoelectrochemical water-splitting system, a photocatalytic layer of TiO_2 film was structured into a Fe_2O_3 photoanode as an interlayer in this study. The photocatalytic interlayer was intended to modify energy bands and facilitate electron transfer to the electron collector in the photoanode; the effectiveness of the interlayer was evaluated from the related UV–vis absorbance and CV data. According to our research's results the photoelectrochemical performance with the TiO_2 interlayer showed a significant improvement in the photocurrent density as well as the onset voltage for photocurrent generation [9]. In our study, the integration of Fe_2O_3 and TiO_2 materials into a PEC cell for performance improvement was carried out with the nano-sized Fe_2O_3 thin layer

supported on a film of tubular shaped TiO_2 nanoparticles. The film of tubular-shaped TiO_2 nanoparticles was fabricated by repetitive self-assembling method. The TiO_2 nanoparticles were converted from hydrogen titanate nanotube (H-TiNT) powders, which had been synthesized by hydrothermal process. Fe_2O_3 samples as a photoanode thin film for water splitting were prepared on H-TiNT (hydrogen-titanate nanotube) film/FTO substrates by simple dipping method in an aqueous $Fe(NO_3)_3$ solution, followed by heat-treatment at temperatures of 420°C to 550°C for 10 min in air, where to prepare H-TiNT layer with a ~700 nm thickness on the FTO substrate, initially, the repetitive self-assembling of oppositely charged ions in an aqueous solution was conducted to directly coat the H-TiNT particles obtained from a hydro-thermal technique on a FTO substrate [10]. The effects of processing parameters of the nanostructured materials such as heat treatment temperature, working environment, processing time, etc. were carefully monitored and investigated in connection with the performance. In addition to the characterization of the photo anode materials, the effect of the each constituent material's location in the multilayered electrodes on the performance was also systemically assessed especially from the microstructure and energy band structure viewpoints.

Synthesis of the samples

Hematite Fe_2O_3 samples were prepared on a transparent conducting substrate of FTO glass (3*3 cm^2) or H-TiNT, by a simple dipping method in aqueous solutions [10]. Repetitive self-assembling of oppositely charged ions in an aqueous solution was applied to coat the H-TiNT powder on the FTO glass, which was obtained from a hydrothermal technique [10, 11]. Before coating of the H-TiNT powder on the FTO glass, the glass was etched for 20 min by using Piranha solution (7:3=conc. H_2SO_4: H_2O_2) to make fresh surface, and the surface was treated for 20 min in 0.2 M polyethylene imine (PEI, Aldrich) aqueous solution containing positively charged ions. All the aqueous solutions were prepared using distilled water of 1.8MΩ. The surface-pretreated FTO glass was immersed for 20 min in an aqueous 10 g/L H-TiNT solution dispersed together with 0.2M tetra butyl ammonium hydroxide (TBAOH, Aldrich) to produce negatively charged ions. Using the same method, an H-TiNT-treated film was subsequently immersed in 0.2 M poly diallyl dimethyl ammonium chloride (PDDA, Aldrich) aqueous solution containing positively charged ions. Repetition of these processes yielded an H-TiNT film coated on the FTO glass with approximately 700~1000 nm thickness [12]. The obtained H-TiNT/FTO glass was dried under UV-Vis light irradiation (Hg-Xe 200W lamp, Super-cure, SAN-EI Electric) to remove water and all the surfactants, such as PEI, TBAOH, and PDDA using photo catalytic removal reaction occurred by H-TiNT particles with the optical energy band gap of 3.5eV, without any sintering. Then, for the Fe_2O_3 nanoparticle coating process on the top of H-TiNT/FTO , the dried H-TiNT/FTO substrates were dipped in an aqueous 1.0M $Fe(NO_3)_3$ solution for 6~24 hrs. It was also done by multiple dipping of the samples in the solution along with the heat-treatment after each dipping, under 600°C for 10 min in air atmosphere. In order to have thin thickness of the Fe_2O_3 film which has a band gap of 2.2 eV, the optical energy band gap of the Fe_2O_3/H-TiNT/FTO samples were controlled to be in the range of 3.24~2.9 eV. The heat-treatment was done inside a box furnace with the heating rate of 500°C/sec to produce the final photo anode thin film with α-Fe_2O_3 phase, where the rapid heating rate was accomplished by plunging the samples into the hot zone of the furnace maintained at 500°C. For formations of H-TiNT top layer on $Fe(NO_3)_3$/FTO films (finally TiO_2/ Fe_2O_3/FTO arrangement), the precursor solution of Fe_2O_3 film supported was made of 1.0 M $Fe(NO_3)_3 \cdot 9H_2O$ and 0.2 M TBAOH (tetra butyl ammonium hydroxide, Aldrich) for dipping fresh FTO substrate for 12 hrs. After that, obtained Fe $(NO_3)_3$/FTO were dried at 80°C for 12 hrs. For formation of H-TiNT/Fe $(NO_3)_3$/FTO films, repetitive self-assembling of oppositely charged ions in an aqueous solution was applied to coat directly the H-TiNT

particles using the same process explained above. All dipping process was carried out at room temperature in air.

Characterization

After the heat-treatment at various conditions, the surface microstructure, crystallinities, optical energy band gap, and I-V electrochemical properties of the samples were analyzed using scanning electron microscopy (SEM; S-4700, Hitachi), Raman spectroscopy (Renishow, inVia Raman microscope), UV-Vis spectroscopy (S-3100, Sinco) and cyclic voltammetry (μAutolab type III, Micro Autolab), respectively. In order To measure the I-V electrochemical property of the working electrodes (e.g., Fe_2O_3, H-TiNT, Fe_2O_3/H-TiNT, H-TiNT/Fe_2O_3 samples) a calomel electrode and a Pt wire were used as the reference and counter electrodes, respectively, in an aqueous 1.0 M NaOH deaerated solution under irradiation of 130 mW/cm^2 UV-Vis spectrum (Hg-Xe 200W lamp, Super-cure, SAN-EI Electric). The measured potentials versus calomel electrode were converted to the reversible hydrogen electrode (RHE) scale.

Results and Discussion

The surface microstructures of samples were shown by SEM microscopic images. In fig 3.1 the Fe oxide and the H-TiNT films coated as a photo anode material on the pure FTO substrate of the samples were observed. Samples were heat-treated under the same conditions of below 600°C for 10 min in the air to transform H-TiNT and Fe $(NO_3)_3$ on the FTO substrate to anatase TiO_2 and hematite-Fe $(NO_3)_3$ phases, respectively [9]. The as-coated H-TiNT thin film in fig 3.2(a) shows that its surface consists of fibrous particles of 100~250 nm in length and about 10 nm in diameter conforming to the contour of the substrate. As the heating temperature increased, the original fibrous shape of the H-TiNT particle became divided into very small and spherical ones while forming a flat and compact surface. Changes in the particle shape with the increasing temperature was coinciding with those of heat-treated H-TiNT powders as reported by Qamar et al [13]. It was also observed that the as coated film of about 700 nm with roughness of ±200 nm before the heat treatment became approximately 150 nm with roughness of ±20~30 nm at 600°C. The results for the heat-treated H-TiNT films can be summarized that the decrease in thickness and the fragmentation of the fibrous particles into smaller particles occurred with the heating temperature increase [14].

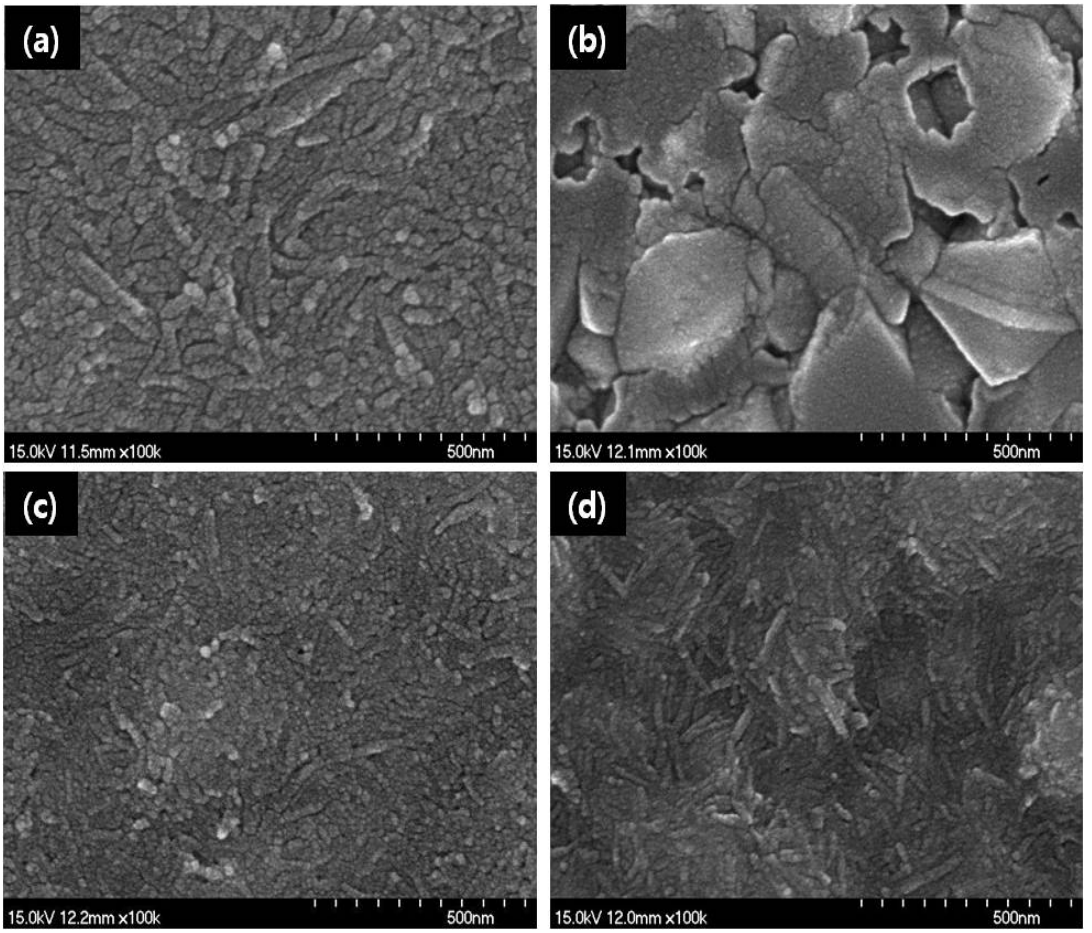

FIGURE 3.1
SEM images of the surface microstructures of films: (a) TiO_2/FTO, (b) Fe_2O_3 (27.16 wt%)/FTO, (c) Fe_2O_3 (65.48 wt%)/TiO_2/FTO, and (d) $Fe_{0.26}Ti_{0.74}O_2$/FTO

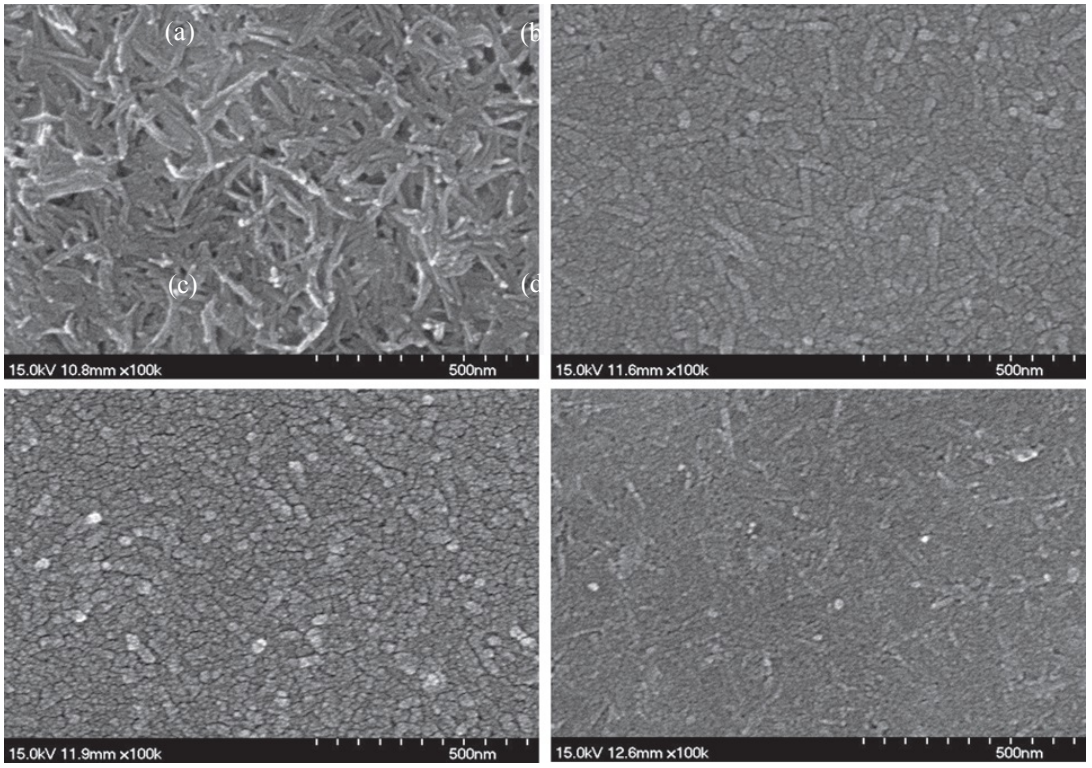

FIGURE 3.2
SEM photographs of the surface microstructures of films heat treated at (b) 500°C, (c) 550°C, and (d) 600°C in air compared with (a) of the as-coated TiNT film

Figure 3.3 displays the SEM images for the surface microstructures of the Fe oxide and the H-TiNT films coated as a photoanode material on the pure FTO substrate, which were all heat treated at 500°C for 10 min in the air. Fig 3.3(a) is the surface of the heat-treated FTO substrate with 300~500 nm sized grains and a roughness of+/- 200nm. Figs. 3.3(b) and (c) are the images of Fe oxide films with 27.16 and 100 wt% of Fe_2O_3, respectively, coated on the surface of the FTO substrate after multiple dips in an aqueous 1 M Fe $(NO_3)_3$ solution, drying, and heat treatment. Here, the amounts of Fe_2O_3 were calculated by multiplying the measured concentration of combined elements of Sn and Fe by energy dispersive spectroscopy, assuming a complete conversion of Fe $(NO_3)_3$ to Fe_2O_3. Fig. 3.3(d) illustrates the H-TiNT film on the FTO substrate obtained by the repetitive self-assembling method as described in the experimental procedure. Fig. 3.3(b) depicts the FTO substrate partially covered with less than 10 nm wide Fe_2O_3 particles. Figs. 3.3(c) and (d) present the FTO substrate fully covered with 10~30 nm sized Fe_2O_3 particles and H-TiNT nanoparticles, respectively. It can be seen in Fig. 3.3(d) that the H-TiNT nanoparticles consist of spherical and longitudinal particles transformed from ~10 nm wide and ~100 nm long tubular shaped particles. It was confirmed by SEM and TEM techniques that the films in Figs. 3.3(c) and (d) have less than 1 μm-thick film coatings, especially Fig. 3.3(d) was 700~1000 thick [15, 11].

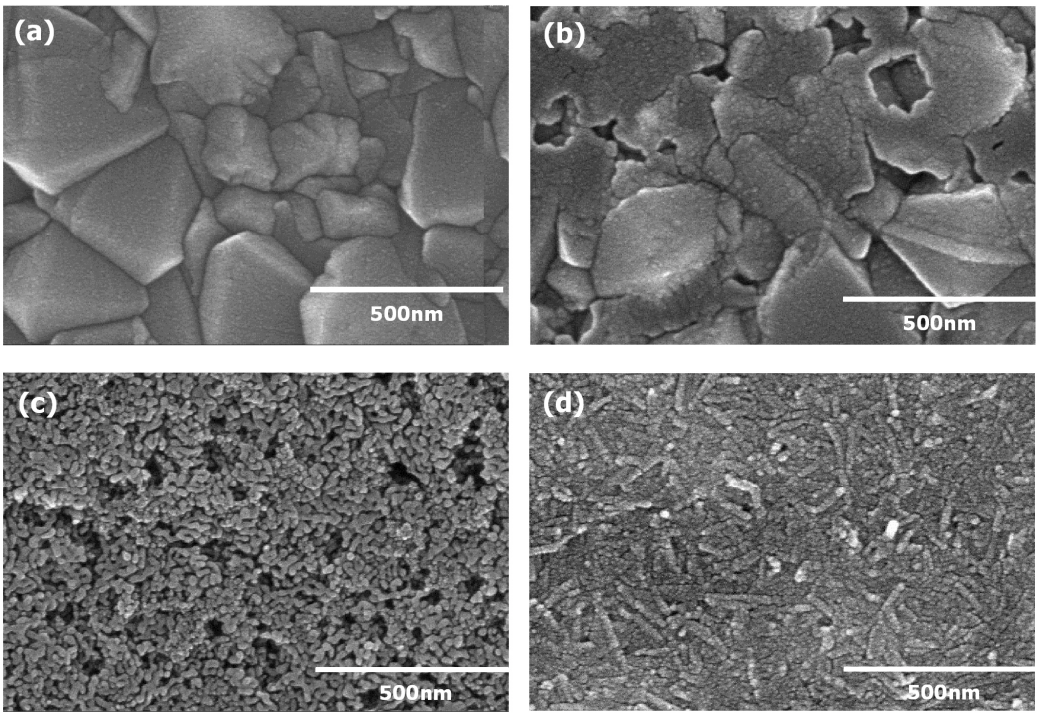

FIGURE 3.3
SEM surface images of Fe oxide and TiNT films coated on the FTO substrate; (a) FTO film, (b) Fe oxide(Fe_2O_3=27.16 wt%)/FTO film, (c) Fe oxide(Fe_2O_3=100 wt%)/FTO film, and (d) H-TiNT/FTO film, which were heat-treated at 500°C for 10 min in air

According to microstructure observed in figure 3.4 it was suggested that film uniformity along with the controlled particles size could play an important role for the performance improvement; Fe_2O_3/TiO_2/FTO sample (figure 3.4(b)) with the best performance consisted of smaller particles with high uniformity than sample (c) of TiO_2/Fe_2O_3/FTO. Double heat treated sample (d) of Fe_2O_3/TiO_2/FTO showed an inferior performance to the corresponding sample (b) with the same layer structure, which was annealed only one time. This result also confirmed the importance of microstructure to the performance; the poor microstructure with agglomerated particles and cracked surface after the double heat treatment as shown in sample (d) adversely affected the performance of the sample. On the other hand, figure 3.4(a) shows the Fe_2O_3 precursor powders becoming much larger when heat treated at 500°C for 10 min, compared to the Fe_2O_3 particles existing together with the TiO_2 in the case of (b)-(d). These observations are consistent with the results of figure 3.18, which showed the restrained growth of the Fe_2O_3 particles by H-TiNT during the heat treatment. It is noteworthy that among the samples with TiO_2 layer, the samples (figures 3.4(b) and (d)) with the TiO_2 layer in between Fe_2O_3 and FTO layer showed better result than the sample (figure 3.4(c)) having the TiO_2 layer above Fe_2O_3 layer. These results were discussed in terms of energy band structure and microstructure [12].

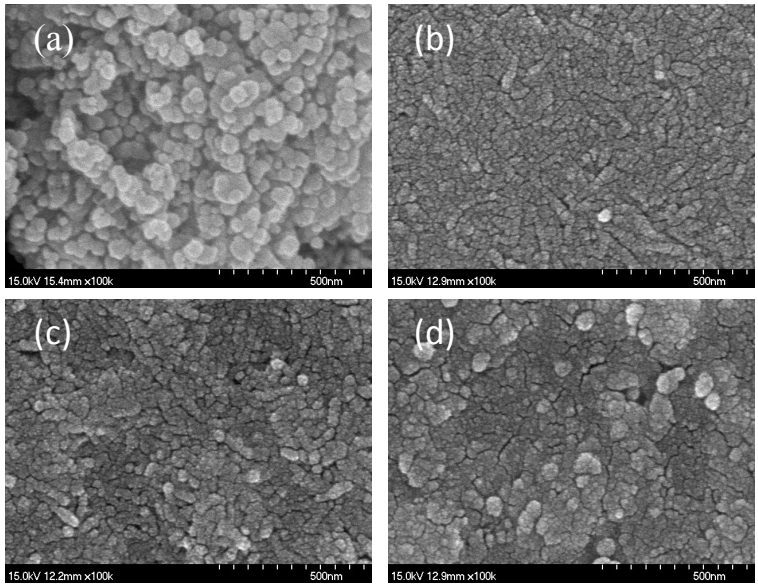

FIGURE 3.4
SEM photos of (a) Fe $(NO_3)_3$ powders heat treated at 500°C for 10 min, and (b), (c), (d) correspond to Figure 3.18 (b) $Fe_2O_3/TiO_2/FTO$, (c) $TiO_2/Fe_2O_3/FTO$, and (d) $Fe_2O_3/TiO_2/FTO$ double heat treated, respectively

These results were discussed in terms of energy band structure and microstructure. Energy band diagrams of the $Fe_2O_3/TiO_2/FTO$ and $TiO_2/Fe_2O_3/FTO$ samples without UV-vis light irradiation were schematically drawn in figures 3.5(a) and (b), respectively. It was proposed by Wang et al. that a photoelectrode with TiO_2 film located above Fe_2O_3 film was a favorable structure for electrons transfer from the energy band diagram consideration [16]. Their claim seems to be reasonable from the comparison of the energy band diagrams when not under UV-vis light. However, our results showed that the electrons generated on the Fe_2O_3 layer in the $Fe_2O_3/TiO_2/FTO$ photoanode could be transferred to the TiO_2/FTO when under the UV-vis light irradiation by overcoming the discontinuity of the conduction bands.

On the other hand, the microstructure of the $Fe_2O_3/TiO_2/Fe_2O_3$ sample synthesized for the current work was also carefully considered. While synthesizing the $Fe_2O_3/TiO_2/FTO$ sample, some of the Fe_2O_3 nanoparticles could be infiltrated to the bottom FTO substrate through TiO_2 particles when TiNT/FTO was placed in the precursor solution of Fe_2O_3. As a result, Fe_2O_3 nanoparticles could also be present in the TiO_2 middle and the bottom FTO layer as depicted in figure 3.5(c). Thus, our sample of $Fe_2O_3/TiO_2/FTO$ seemed actually to have an energy band diagram combining both of figures 3.5(a) and (b), indicating that the photoanode with Fe_2O_3 nanoparticles present even in the middle and bottom substrate is preferable for the performance enhancement.

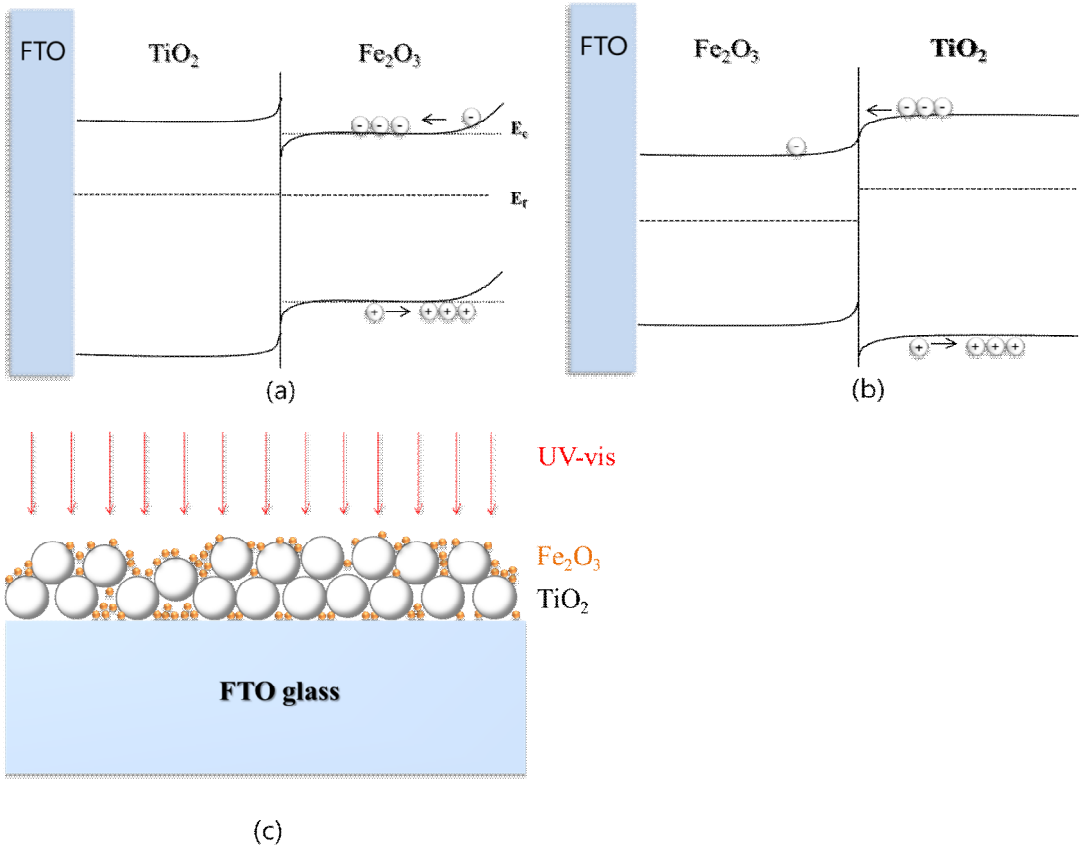

FIGURE 3.5
Energy band diagrams of (a) $Fe_2O_3/TiO_2/FTO$ and (b) $TiO_2/ Fe_2O_3/FTO$ photoanode, and (c)schematic microstructure of Fe_2O_3-TiO_2-FTO

The Raman spectra has been shown in fig 3.6 to confirm the phase or crystallinity of the samples in fig 3.3(a), 3(c), and 3(d) [14]. The crystallographic characteristics of heat-treated FTO, Fe_2O_3, and H-TiNT films were also compared with those of the untreated FTO film (not shown). It could be observed as shown in Fig. 3.6 that spherical α-Fe_2O_3 phase and main longitudinal titanate phase with a minor phase of spherical anatase TiO_2 phase, respectively, on the surface, with compared to that of our previous report [14].

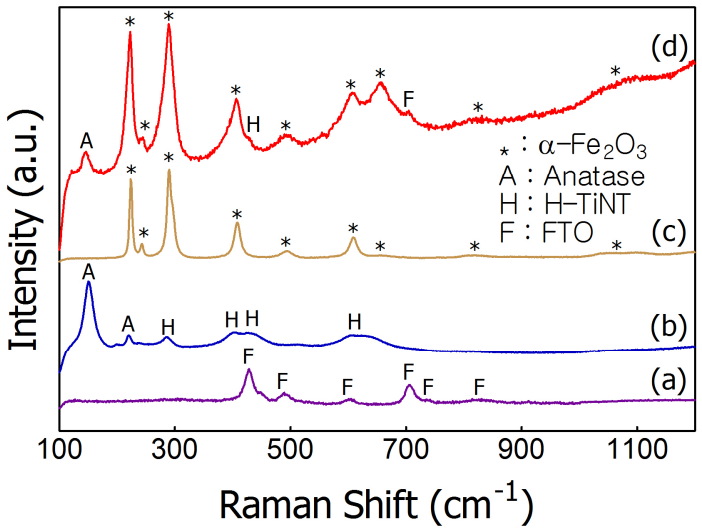

FIGURE 3.6
Raman spectra of (a) FTO, (c) Fe_2O_3/FTO and (d) Fe_2O_3/H-TiNT/FTO film, which were heat-treated at 500°C for 10 min in air, comparing with that of (b) H-TiNT/FTO heat-treated at the same condition

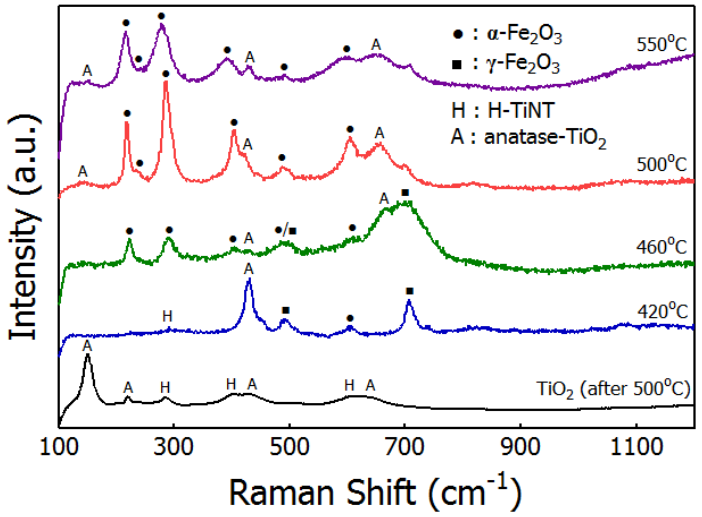

FIGURE 3.7
Raman Spectroscopy of Fe_2O_3 films heat-treated at same temperatures applied for the samples described in Figure 3.9

Figure 3.7 displays Raman spectroscopy data for the Fe_2O_3. Samples were heat treated for 10min at the same temperatures applied for the samples ((a) FTO at 500°C, (b) Fe_2O_3/FTO at 500°C, (c) Fe_2O_3/TiO_2/FTO at 420°C, (d) Fe_2O_3/TiO_2/FTO at 460°C, (e) Fe_2O_3/TiO_2/FTO at 500°C, (f) Fe_2O_3/TiO_2/FTO at 550°C) described in fig 3.9 to monitor phase changes during heat treatment. Fe_2O_3 was identified to be γ-Fe_2O_3 phase after heat treatment at 420°C. It gradually transformed into α-Fe_2O_3 phase through heat treatment at the higher temperatures. On the other hand, the phase change of TiO_2 located under

Fe_2O_3 layer was described in our previous works [10]; as-coated H-TiNT particles were transformed gradually into anatase-TiO_2 phase as the heating temperature increased, finally fully transforming to anatase-TiO_2 phase at higher temperatures than 500°C. Based on the phase change observations, phase of Fe_2O_3 seems to not affect much on the performance improvement of the photo electrode as shown in fig 3.9. But the performance was likely to be more strongly affected by the phase of TiO_2; mixed phases of H-TiNT and anatase-TiO_2 at 500°C showed best result rather than TiO_2 phase only at the temperatures higher than 500°C [10].
As it has been shown in fig 3.8 during the LBL-SA process, the H-TiNT particles were coated on the FTO glass as a porous form without changing in its phase. Then they were transformed gradually into anatase TiO_2 phase, finally fully transforming at more than 500°C. This transformation behavior at below 600°C has been confirmed to agree with that of the particles in the powder [7]. As presented in fig 3.8 (d) and (e), the anatase TiO_2 phase showed a gradual increase in intensities of 150, 201, 400, 519, and 644 cm−1 corresponding to its Raman characteristics at 550°C or more. Therefore, with increasing in heating temperature, the as-coated fibrous H-TiNT particles on the FTO glass were divided into small particles of 10∼20 nm in diameter with forming a perfect anatase TiO_2 phase with the flat and compact surface [14].

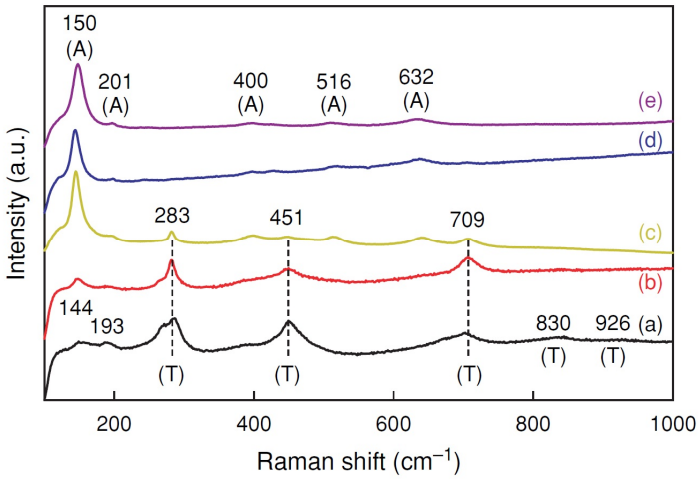

FIGURE 3.8
Raman spectra of TiNT films after heat treatment at (b) 400°C, (c) 500°C, (d) 550°C, and (e) 600°C in air compared with (a) of the as-coated TiNT thin film

The I-V PEC data of the samples measured under 100 mW/cm^2 of UV-Vis light illumination, in which the linear sweep voltammetry was in the range of +0.4 - +2.0 V vs. the RHE. According to fig 3.9, sample (a) FTO and (b) Fe_2O_3/FTO correspond to FTO substrate only and Fe_2O_3 coated on the FTO, respectively. Samples (c)-(f) were heat treated at the predetermined temperatures with TiO_2 layer inserted in between Fe_2O_3 and FTO substrate. The onset voltage for the initiation of photocurrent flow decreased from 0.89 to 0.75 V vs. RHE with the heat treatment temperature of up to 500°C. The photocurrent density at 1.23 V vs. RHE also showed a gradual improvement from 1.87 to 4.65 mA/cm^2 with the heating temperature of up to 500°C. However, the performance of the photo electrode deteriorated after heat treatment at 550°C as observed with the sample (f). To investigate the sources for the performance improvement/deterioration of the samples with the heating temperature, phase/morphology changes and impedance variations were studied in the followings [20].

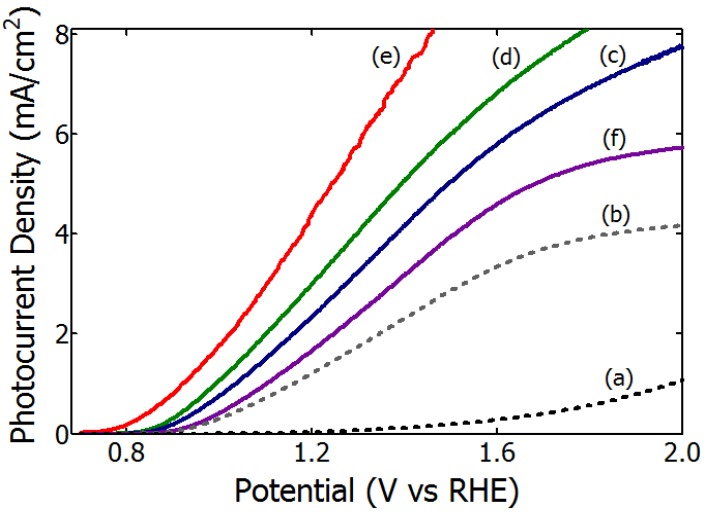

FIGURE 3.9
I-V PEC characteristic of the heat-treated films for 10 min in air. Sample (a) FTO at 500°C, (b) Fe_2O_3/FTO at 500°C, (c) Fe_2O_3/TiO_2/FTO at 420°C, (d) Fe_2O_3/TiO_2/FTO at 460°C, (e) Fe_2O_3/TiO_2/FTO at 500°C, (f) Fe_2O_3/TiO_2/FTO at 550°C

As it has been seen in fig 3.10 for the application of H-TiNT or TiO_2 thin films to water splitting, their electrochemical characteristics were evaluated using a linear sweep voltammetry in the short range of 1.5~2.0 V. The as-coated (a) and heat-treated (not shown) H-TiNT films without UV-A irradiation had very small currents of 12.5 μA/cm^2 and 10~30 μA/cm^2 at 2.0 V, respectively. However, the current of the films continued to increase as the temperature increased, showing a maximum value of 184 mA/cm^2 at 2.0 V at 500°C and then decreasing gradually at higher temperatures. These changes in the current at a heating temperature of up to 500°C are mainly caused by the decrease in film resistance and in the porosity and transformation of anatase from the H-TiNT phases. At a higher temperature, these changes are caused by an increase in the interfacial electro-chemical resistance related to the contact characteristics between electrode and electrolyte. Therefore, the H-TiNT/TiO_2 film with mixed phases obtained at 500°C can be suggested to be appropriate for the water splitting electrode [14].
As it has been seen in fig 3.10 for the application of H-TiNT or TiO_2 thin films to water splitting, their electrochemical characteristics were evaluated using a linear sweep voltammetry in the short range of 1.5~2.0 V. The as-coated (a) and heat-treated (not shown) H-TiNT films without UV-A irradiation had very small currents of 12.5 μA/cm^2 and 10~30 μA/cm^2 at 2.0 V, respectively. However, the current of the films continued to increase as the temperature increased, showing a maximum value of 184 mA/cm^2 at 2.0 V at 500oC and then decreasing gradually at higher temperatures. These changes in the current at a heating temperature of up to 500oC are mainly caused by the decrease in film resistance and in the porosity and transformation of anatase from the H-TiNT phases. At a higher temperature, these changes are caused by an increase in the interfacial electro-chemical resistance related to the contact characteristics between electrode and electrolyte. Therefore, the H-TiNT/TiO2 film with mixed phases obtained at 500oC can be suggested to be appropriate for the water splitting electrode [14].

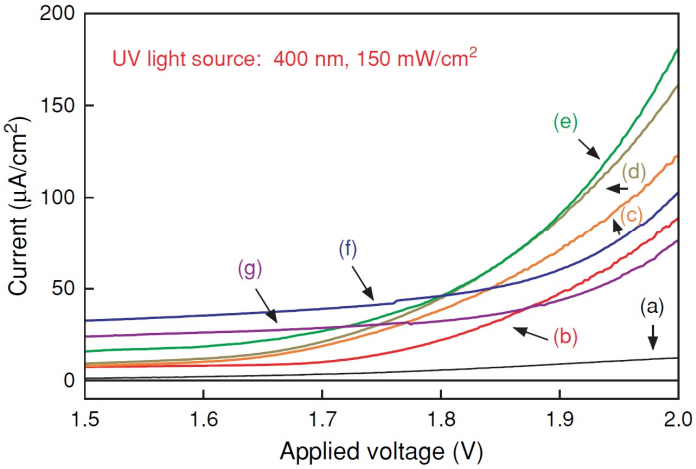

FIGURE 3.10
I–V curves of TiNT films after heat treatment at (b) as-prepared TiNT film, (c) 400°C, (d) 450°C, (e) 500°C, (f) 550°C, and (g) 600°C in air compared with that (a) of as-coated TiNT thin film (dark reaction)

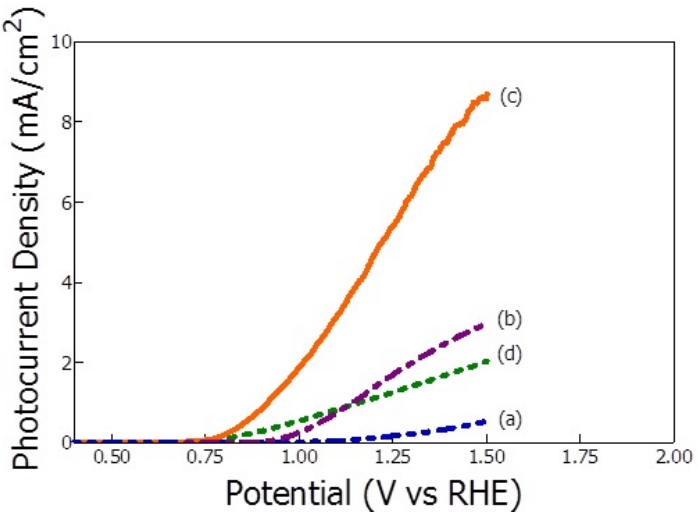

FIGURE 3.11
I-V photo electrochemical characteristic of the films: (a) TiO_2/FTO, (b) Fe_2O_3 (27.16 wt%)/FTO, (c) Fe_2O_3 (65.48 wt%)/TiO_2/FTO, and (d) $Fe_{0.26}Ti_{0.74}O_2$/FTO

In figure 3.11 the I-V photo electrochemical characteristics of the samples were measured to observe the effect of the TiO_2 interlayer in the Fe_2O_3-based photo anode in the 1 M NaOH solution. The linear sweep voltammetry was in the range of 0.0 to +1.5 (V vs RHE) under 100 mW/cm^2 UV-vis light illumination. Samples of TiO_2 [Fig. 3.11 (a)] and Fe_2O_3 [Fig. 3.11 (b)] films coated on the FTO substrate were measured as the reference data. It should be mentioned that the Fe_2O_3 film coated on the FTO substrate showed some variation in the photocurrent as a function of Fe_2O_3 wt%; the best result is shown here with about 27.16 wt% Fe_2O_3, and the other data for different amounts of Fe_2O_3 are

presented in Fig. 3.12(b). In the case of Fig. 3.11 (d), the sample was prepared by an ion-exchange method between Fe and H in the H-TiNT, in which the onset voltage shifted to a lower value, as expected, owing to the catalytic effect of TiO_2. However, the photocurrent density was observed to still be lower, at an applied voltage above 1.17 (V vs RHE), than the sample made of Fe_2O_3 only [Fig. 3.11 (b)].

The sample in the case of Fig. 3.11 (c) was fabricated with the TiO_2 interlayer inserted between the Fe_2O_3 layer and the FTO substrate. The amount of Fe_2O_3 was varied to obtain a high photocurrent by minimizing the recombination. Part of the TiO_2 interlayer was also exposed to the electrolyte to utilize the catalytic effect of TiO_2, by adjusting the amount of Fe_2O_3 coated on the top of the interlayer, as shown in Fig. 3.1 (c). The amount of Fe_2O_3 was optimized at 65.48 wt% on the basis of the performance data as a function of Fe_2O_3 amount, as shown in Fig. 3.12. The I-V curve for the Fe_2O_3/TiO_2/FTO sample with 65.48 wt% Fe_2O_3 coverage is shown in Fig. 3.11 (c). It is worth noting that the optimal amount of Fe_2O_3 for the photocurrent performance depended strongly on the material structure, as shown in Fig. 3.12, where the Fe_2O_3/FTO sample yielded the best result at 27.16 wt% of Fe_2O_3.

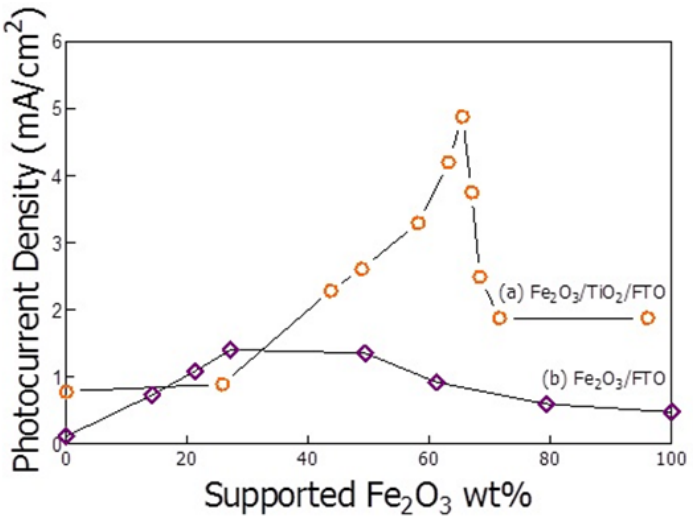

FIGURE 3.12
Onset voltage values from I-V photo electrochemical characteristic curves (color) as a function of wt% Fe2O3 on (a) TiO2/FTO and (b) FTO substrates

Among the samples in Fig. 3.11, the sample with the TiO_2 interlayer [Fig. 3.11 (c)] showed a significantly improved performance in terms of the onset voltage and photocurrent density: the onset voltage became close to the theoretical value of 0.4 V reported by Tilley et al [18] and the current density markedly increased to 4.35 mA/cm^2 at 1.23 (V vs RHE). It can be thought that the reduction in overvoltage is due to the diffusion of Fe into the TiO_2 layer during the heat treatment specified in the experimental procedure. A similar result was observed for the sample in the case of Fig. 3.11 (d), in which $Fe_xTi_{1-x}O_2$ (x=0.26) was formed by ion exchange and the subsequent heat treatment. The marked photocurrent density increase in Fig. 3.11 (c) was thought to be achieved mainly by two means: 1) the optimization of the thickness (amount) of Fe_2O_3 to minimize recombination (Fig. 3.12) as well as maximize the photo energy absorption, and 2) the insertion of the TiO_2 interlayer to efficiently transfer

electrons to the FTO electron collector by modifying energy bands, the concept of which was previously suggested by Hattori et al [19].

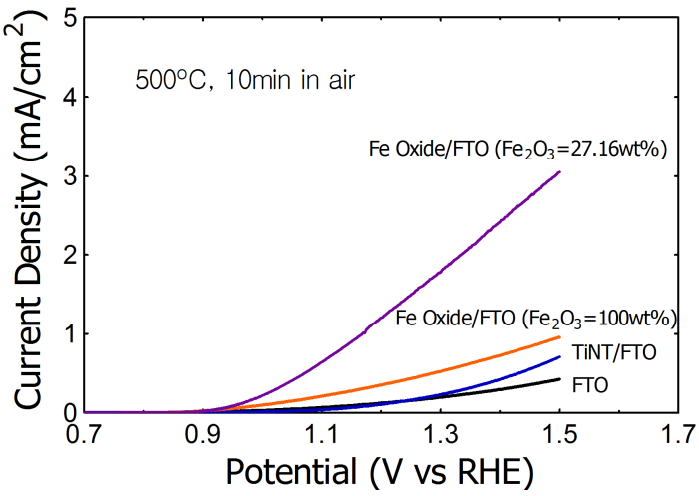

FIGURE 3.13
I-V characteristic curves for FTO film, and H-TiNT/FTO and Fe oxide (Fe_2O_3 with 27.16 and 100 wt%)/FTO films

On the other hand the specimens in Fig. 3.3 were initially applied to the photo anode for the water splitting process, where their I-V electrochemical characteristics were evaluated using a linear sweep voltammetry in the range of +0.7 ~+1.5 V versus the RHE under 130 mW/cm^2 UV-Vis light illumination (Fig. 3.13). The current signals of all the specimens were detected with an onset voltage of around 0.9 V versus RHE. Both the heat-treated FTO and H-TiNT/FTO films yielded relatively very low currents up to the applied potential of 1.3 V versus the RHE, indicating that water splitting is electrochemically difficult at 1.23 V versus RHE. When the Fe_2O_3 film partially covered the FTO substrate (Fe_2O_3=27.16 wt%), its current significantly increased (1.39 mA/cm^2) at 1.23 V versus RHE, whereas the Fe_2O_3 film, which fully covered the surface of the FTO substrate, yielded a relatively low value, although higher than those of the heat-treated FTO and H-TiNT/FTO films. This variation indicates that not all the currents generated by the thick or full Fe_2O_3 film coating can be completely collected through the FTO conducting layer, compared with those generated by the thin or partial Fe_2O_3 film coating. As shown in Figs 3.3(b) and (c), it is thought that the collection of electrons in these specimens was not perfectly accomplished by the 5~30 nm Fe_2O_3 particles due to the typical recombination of electron-hole [10, 17], although the amount of generated electrons on the thick or full Fe_2O_3 film coating on the FTO substrate with UV-Vis light irradiation could become ample enough. Thus, it is obviously known that the amount or size of the Fe_2O_3 particles supported on the FTO substrate should be appropriately controlled to increase the current. However, because it was found that the current decreased abruptly with the Fe_2O_3 more than 27.16 wt% as in our preliminary experiments, our focus should be directed to the reduction of the Fe_2O_3 particle size or the insertion of a new easy path layer to the FTO substrate beneath the Fe_2O_3 film for energy band alignment. It would be more effective to protect the recombination of electrons and holes photo-generated in real system. Various amounts of Fe_2O_3 nanoparticles were supported on an H-TiNT/FTO composite film using the self-assembling or dipping procedure, as shown in Fig. 3.14.

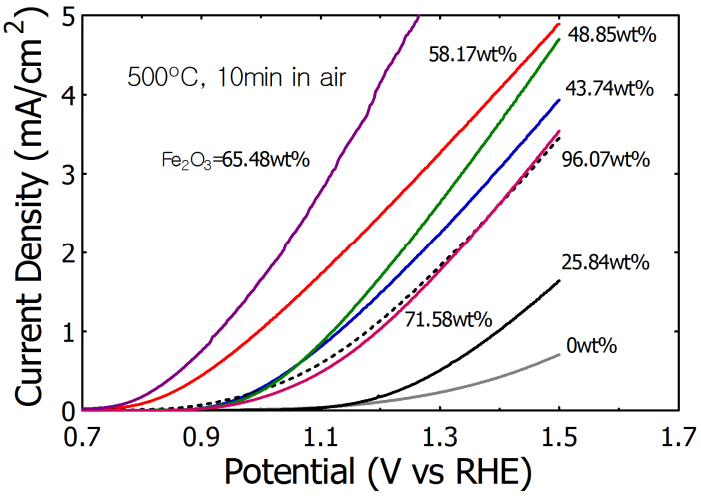

FIGURE 3.14
I-V characteristic curves for Fe_2O_3 films with various amounts of 0~100 wt% supported on H-TiNT/FTO film, followed by heat-treatment at 500°C for 10min in air. Here, 0 wt% means that there are no Fe_2O_3 particles on H-TiNT/FTO film and 100 wt% means Fe2O3 particles covered fully on the surface of the film

Figs. 3.14 and 15 showed the I-V electrochemical characteristics curves and the current at 1.23 V versus RHE, with varied Fe_2O_3 amounts supported on an H-TiNT/FTO composite film by controlling the dipping time or multiple dippings in an aqueous Fe $(NO_3)_3$ solution, respectively. This was followed by heat-treatment at 500°C for 10 min in air to obtain the hematite-Fe_2O_3 phase. Here, the amount of Fe_2O_3 was also calculated by multiplying the measured concentration of combined elements of Ti and Fe by energy dispersive spectroscopy, assuming a complete conversion of TiO_2 and Fe_2O_3 from H-TiNT and Fe $(NO_3)_3$. As the supported amount of Fe_2O_3 nanoparticles increases, the onset voltage decreases to approximately 0.7 V versus RHE, whereas their generated current significantly increases. The current density increase can be easily understood by the reasoning that more Fe_2O_3 involved due to the advantage of TiO_2 in the sample would enhance the visible light absorption. Performance improvements were similarly observed with the integrated materials, for the same purpose as ours, such as Fe-modified TiO_2 nanotubes [20] and CuS/ZnS porous nano sheets [21]. As shown in Fig. 3.15, the current at 1.23 V versus RHE peaks at 4.81 mA/cm^2 with 65.48 wt% of the supported Fe_2O_3 nanoparticles on the H-TiNT/FTO film, which is about three-fold as much current as the Fe_2O_3/FTO film. The generated current then decreases abruptly and would become saturated to approximately 1.4 mA/cm^2 due to formation of thick Fe_2O_3 film [11].

For investigating about the effect of the amount of Fe_2O_3 coated on the FTO film I-V photo electrochemical data were also measured in the 1.0 M NaOH solution. The linear sweep voltammetry was in the range of 0.0 - +2.0 (V vs. RHE) under 100 mW/cm^2 of UV-Vis light illumination. Photocurrent density was obtained from the comparison of 'dark' and 'illumination' data. Overall, the photocurrent density of the samples was observed to gradually increase with the amount of Fe_2O_3 until 27.16 wt% Fe_2O_3, beyond which it decreased. It can be deduced from this result that the thickness (or amount) of Fe_2O_3 should be thick enough to effectively absorb photon energy but needs to be controlled to prevent the recombination of electron-hole pairs. Thus the thickness (or amount) of the photo absorbing material of Fe_2O_3 particles needs to be optimized for effective photoelectron absorption without too much recombination of the electron-hole pairs [22, 23].

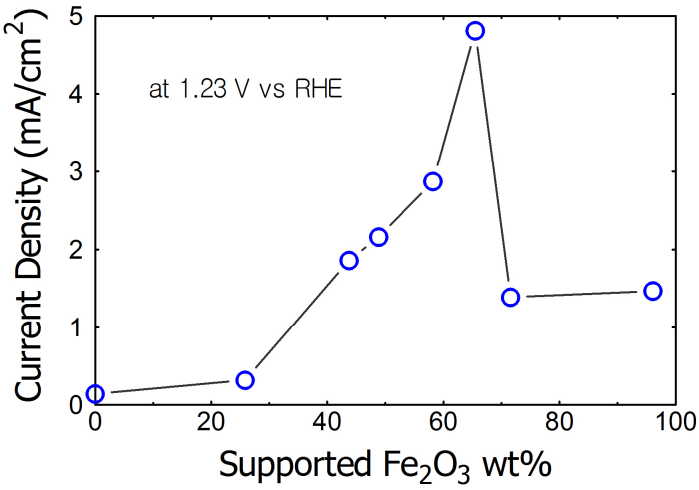

FIGURE 3.15
Current at 1.23V vs RHE from I-V electrochemical characteristic curves of Figure 3.14

For the effective performance of the Fe_2O_3-based photo anode, the microstructure was modified by a surfactant and heat-treatment for performance enhancement. Fig.3.16 (A) shows the morphology of the Fe_2O_3/FTO samples where the Fe_2O_3 precursor particles, already treated with TBAOH surfactant, were heat-treated at various temperatures of 420°C, 500°C, 600°C, and 700°C for 10 min in air, with the heating rate of the selected temperature/sec. Here, the heating rate of the selected temperature/sec was assumed to be obtained by placing the sample instantly in the furnace which had been maintained at the predetermined temperatures well in advance. This assumption seemed to be reasonable considering the nano-scale of the particles and the corresponding films. Careful observation of the microstructure of the samples indicated that 500°C was an optimum heat-treatment temperature in terms of the uniform dispersion of the particles and for maintaining nano-scaled particle size. Below 500°C, the particles were observed to be agglomerated during transition to Fe_2O_3 phase. On the other hand, the particles heat treated at above 500°C, seemed to undergo a thermally activated growth and coalescence into larger ones.

The effect of the TBAOH surfactant can be also investigated for the samples with and without surfactant treatment, which underwent the same heat-treatment. The particles treated with TBAOH were observed to be more uniformly dispersed on the substrate (Fig.3.16 (A) - (b)).The photocurrent densities of the samples described in Fig.3.16 (A) were measured as a function of potential (V vs. RHE) (Fig.3.16 (B)). As expected, the sample processed with TBAOH surfactant and heat-treatment at 500°C, showed the best result among them: the photocurrent density was about 1.32 mA/cm^2 at 1.23 (V vs. RHE) which was about a 32 % improvement compared with 0.96 mA/cm^2 of the sample not surfactant treated.

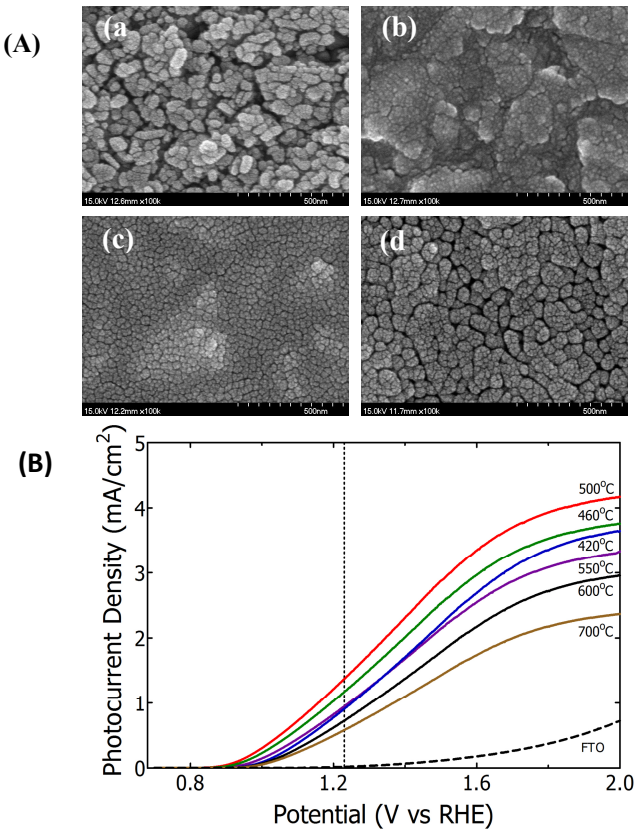

FIGURE 3.16
(A) SEM surface images of the Fe_2O_3 coated on the FTO films, which were treated by TBAOH surfactant and heat-treated at various temperatures for 10 min in air: (a) 420°C, (b) 500°C, (c) 600°C, and (d) 700°C for 10 min. (B) I-V photo electrochemical characteristics curves of Fig.3.16 (A)

The effect of the heating rate and duration period at the heat-treatment temperature on the microstructure and performance of the Fe_2O_3 (TBAOH treated)/FTO electrode is shown in Fig.3.17. Both lower heating rate (0.3°C/sec vs. 500°C/sec) and longer duration time (1 hr at 500°C vs. 10 min at 500°C) were found to cause agglomeration and growth of the Fe_2O_3 particles, which would deteriorate the performance of the photo electrode. Microstructures in Fig.3.17 (A)-(a) and-(b) correspond to the lower heating rate and longer duration time, respectively. For comparison, the microstructure heat-treated at 500°C for 10 min with the heating rate of 500°C/sec can be referenced in Fig.3.16 (A)-(b). The performance of the photo electrode heat-treated under different conditions is compared in Fig.3.17 (B). As expected from the microstructure observations, rapid heating and short duration time produced a favorable microstructure, resulting in better performance. For instance, the photo electrode heat-treated at 500°C for 10 min with the heating rate of 500°C/sec showed more than 1.5 times better performance than that heat-treated at 500°C for 1 hr with the same heating rate [24].

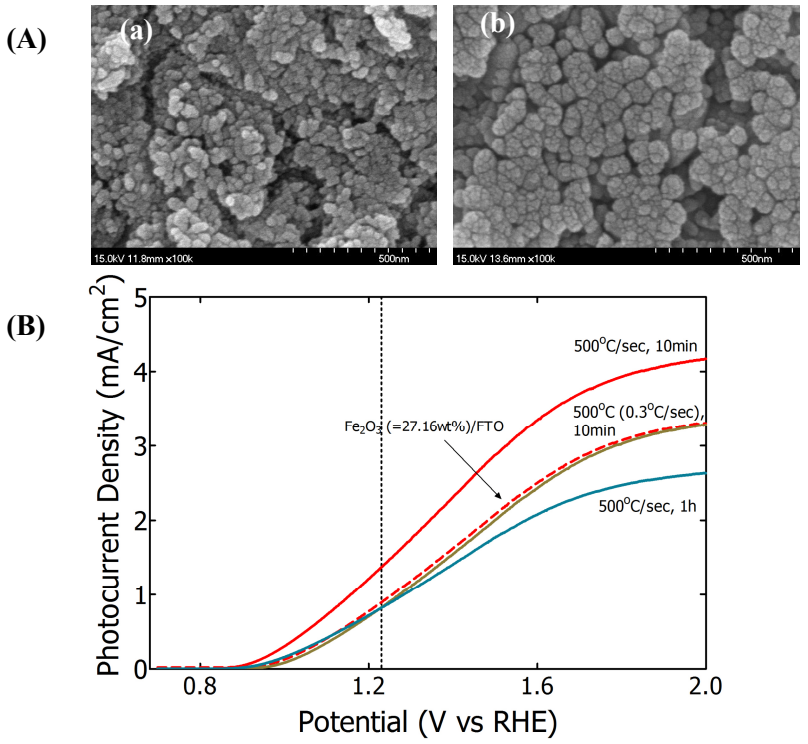

FIGURE 3.17
(A) SEM surface images of the Fe_2O_3 (treated by TBAOH) coated on the FTO films which were heat-treated with a various heating rate in air: (a) at 500°C for 10 min with the heating rate of 0.3°C /sec and (b) at 500°C for 1 hr with the heating rate of 500°C /sec. (B) I-V photo-electrochemical characteristics curves of Fig.3.17 (A), including the sample in Fig.3.16 (B) heat treated at 500°C for 10 min with the heating rate of 500°C /sec

I-V photo electrochemical data and surface morphology of the Fe_2O_3 precursor/(H-TiNT)/FTO samples also has been shown in fig 3.18, which had been heat treated at the predetermined temperatures of 420 ~ 550°C for 10min. The amount of Fe_2O_3 in the samples was 65.48 wt % for the Fe_2O_3/H-TiNT/FTO and about 30 wt% for the Fe_2O_3/FTO, which was determined based on the I-V photo electrochemical performance as reported in our previous study. All the samples were measured in the 1.0 M NaOH solution under 100 mW/cm^2 of UV-Vis light illumination, and the linear sweep voltammetry was in the range of 0.0 ~ +2.0 (V vs RHE). The photocurrent densities were obtained by eliminating the 'dark' fraction from 'illumination' data, where dark data was measured in the dark room without UV light illumination. For the comparison, sample (e) without TiO_2 interlayer was adopted from our previous work.

Regardless of the heat treatment temperatures, the performance improvement was observed in the samples with TiO_2 interlayer incorporated in between Fe_2O_3 and FTO. In particular, sample (c) prepared under the same condition as sample (e) other than the presence of TiO_2 interlayer film showed about 3 times increase of photocurrent density at 1.23 (V vs RHE) and the reduction of the onset voltage to about 0.75 V. These results suggest that the TiO_2 interlayer can play a significant role in the efficient collection and conversion of photo energy. The extent of performance improvement was found to be affected by the heat-treatment temperature; it showed a gradual improvement with the heat

treatment temperature of up to 500°C, above which it rather deteriorated. A similar result was observed with the Fe_2O_3/FTO samples without TiO_2 interlayer film.

Morphology of the Fe_2O_3/FTO sample after heat treatment at 500°C for 10 min was shown in figure 3.18(e) The Fe_2O_3 particles were observed to form a film conformal to the FTO substrate, indicating a very thin and uniform film as noted by Oh et al [9]. Microstructure changes of the Fe_2O_3 precursor/H-TiNT/FTO samples were also monitored as a function of heat treatment temperature of 420 ~ 550°C. The as-coated porous and rough H-TiNT particles with fibrous morphology as reported in our previous work [14] were broken into spherical particles through the heat treatments. It is noteworthy that the Fe_2O_3 particles in the Fe_2O_3/H-TiNT/FTO samples were relatively smaller than those in the Fe_2O_3/FTO sample, suggesting that the growth of the Fe_2O_3 particles was restrained by H-TiNT during the heat treatments. However, no noticeable microstructural differences were observed among the Fe_2O_3/H-TiNT/FTO samples which could explain the performance variation occurred in the samples [12].

Effect of the coating layers arrangement in the Fe_2O_3-TiO_2-FTO samples was investigated in terms of the performance in figure 3.19, in which the photocurrent densities were obtained by eliminating the 'dark' fraction from 'illumination' data, All the samples except sample (d) were heat treated once at 500°C for 10 min in the air following synthesis of the multilayered electrodes. Sample (d) was heat treated twice under the same condition mentioned above; once after TiNT coating on the FTO, then repeated after Fe_2O_3 coating on the heat treated TiO_2/FTO layer. Regardless of the location of TiO_2 layer, above or below Fe_2O_3 layer (Fe_2O_3/TiO_2/FTO: figure 3.19(b) and (d) or TiO_2/Fe_2O_3/FTO: figure 3.19(c)), samples containing TiO_2 layer (figures 3.19(b), (c), and (d)) showed much better performance compared to that (figure 3.19(a)) of without TiO_2 layer; increased photocurrent density as well as reduced onset voltage [12].

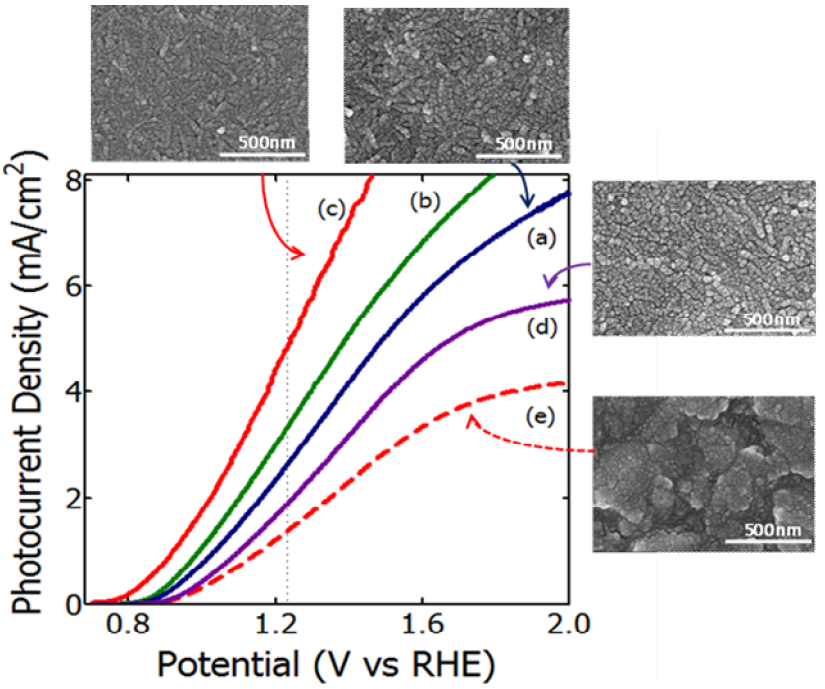

FIGURE 3.18

Photo electrochemical I-V characteristics of Fe_2O_3 precursor/H-TiNT/FTO heat-treated at (a) 420°C, (b) 460°C, (c) 500°C, and (d) 550°C in the air, compared to (e) Fe_2O_3 precursor/FTO heat treated

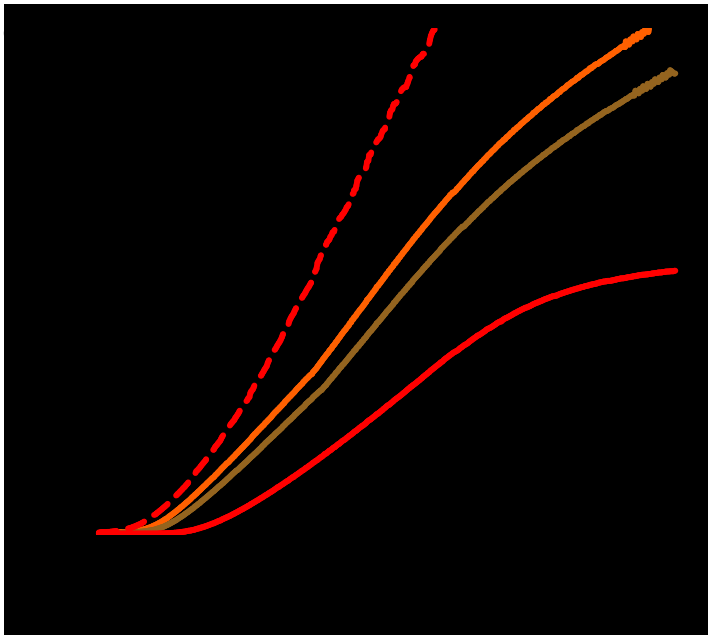

FIGURE 3.19
Photo electrochemical I-V characteristics of the samples with the stacking structures of (a) Fe_2O_3/FTO, (b) Fe_2O_3/TiO_2/FTO, and (c) TiO_2/Fe_2O_3/FTO, which were all heat treated at 500°C for 10 min in the air. Curve (d) was obtained from Fe_2O_3/TiO_2/FTO double heat treated under the same condition as above; 1st after H-TiNT coating on FTO, and 2nd after Fe_2O_3 coating on the heat treated H-TiNT/FTO

CV curves show the oxidation-reduction characteristics of the samples. According to fig 3.20 the FTO, Fe_2O_3/FTO, TiO_2/FTO film do not show any noticeable oxidation-reduction peaks even under UV-Vis light illumination. On the other hand, the Fe_2O_3/TiO_2/FTO film, showed several clear peaks under UV-Vis light. The multiple observed peaks seem to be due to the multilayer effect of the samples. Among the heat-treated samples, Fe_2O_3/TiO_2/FTO sample heat-treated at 500°C showed most distinctive peaks and smallest hysteresis loss. This sample also showed best I-V result as observed in Fig. 3.9 [17].

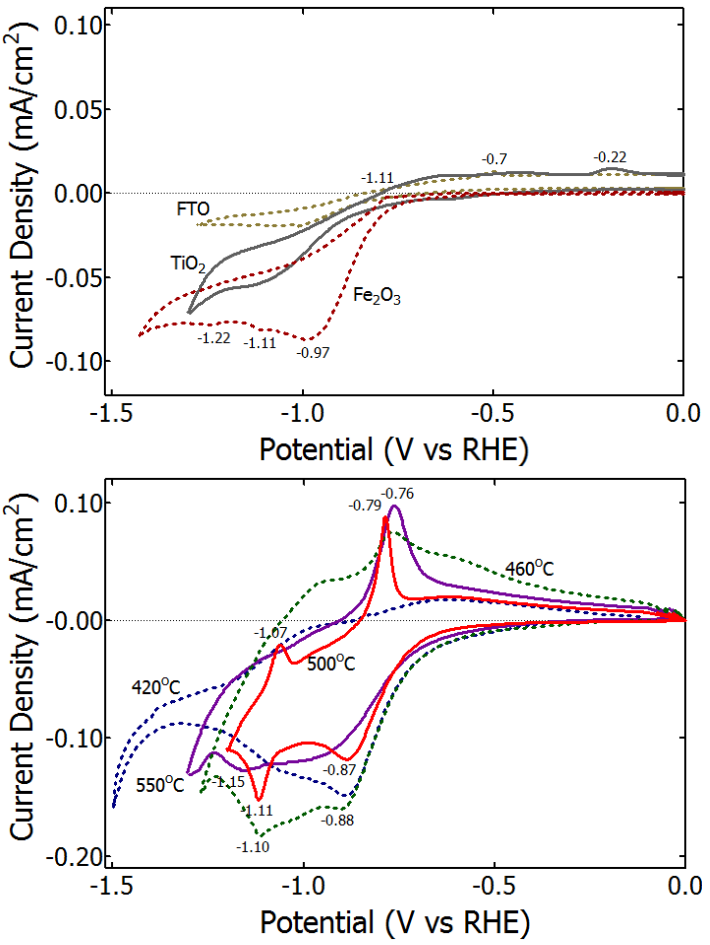

FIGURE 3.20
CV results of base films and Fe_2O_3/TiO_2/FTO films for heat treated 420°C to 550°C under UV-Vis light

Fig. 3.21 expressed impedance and phase were changed as a function of frequency of the samples that were used in Fig. 3.9. Impedance was changed of the samples in Fig. 3.21(a) were consistent with the I-V results in Fig. 3.9; at lower frequency range the impedance was decreased with heat-treatment temperature of up to 500°C. And the effect of TiO_2 interlayer can also be clearly shown; the samples with TiO_2 interlayer has had smaller impedance. Phase shift at low frequency (Fig. 3.21(b)) showed a distinctive difference among samples due to the capacitive element by the existence of TiO_2 interlayer; the catalytic interlayer facilitates the electrons transfer within the electrode. A similar phenomenon was observed in the electrode with the applied potential difference; more phase shift occurred with higher potential applied [17].

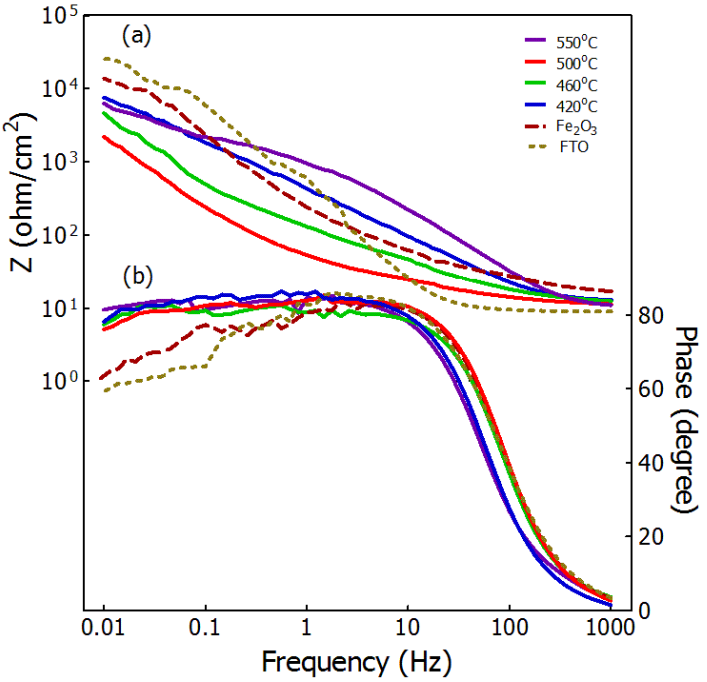

FIGURE 3.21
Bode plot for the samples that were used in Fig. 3.8

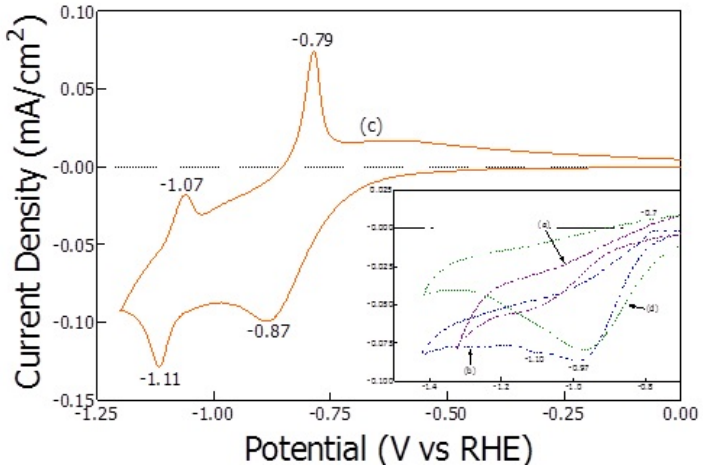

FIGURE 3.22
C-V photo electrochemical characteristic of the films under UV-vis light illumination: (a) TiO_2/FTO, (b) Fe_2O_3 (27.16 wt%)/FTO, (c) Fe_2O_3 (65.48 wt%)/TiO_2/FTO, and (d) Fe0.26Ti0.74O2/FTO

In fig 3.22 the representative oxidation-reduction characteristics of the Fe_2O_3/TiO_2/FTO photo anode have been also shown and compared with others by using CV data. The TiO_2/FTO film did not have appreciable oxidation-reduction peaks, as expected, even under UV-vis light illumination. On the other

hand, the Fe_2O_3/TiO_2/FTO film showed distinctive and strong multiple peaks under UV-vis light, which was also much different from the case of the dark condition observed in our preliminary work, where it did not show any strong or conspicuous peaks. Many of the peaks observed seemed to be caused by the multilayered structure of the sample, particularly the oxidation peak at -1.07 (V vs RHE) that probably occurred at the interfacial combination of Fe_2O_3 and TiO_2, while the other three peaks were similarly observed in the sample of Fe_2O_3 (27.16 wt%)/FTO [Fig. 3.22(b)] [9].

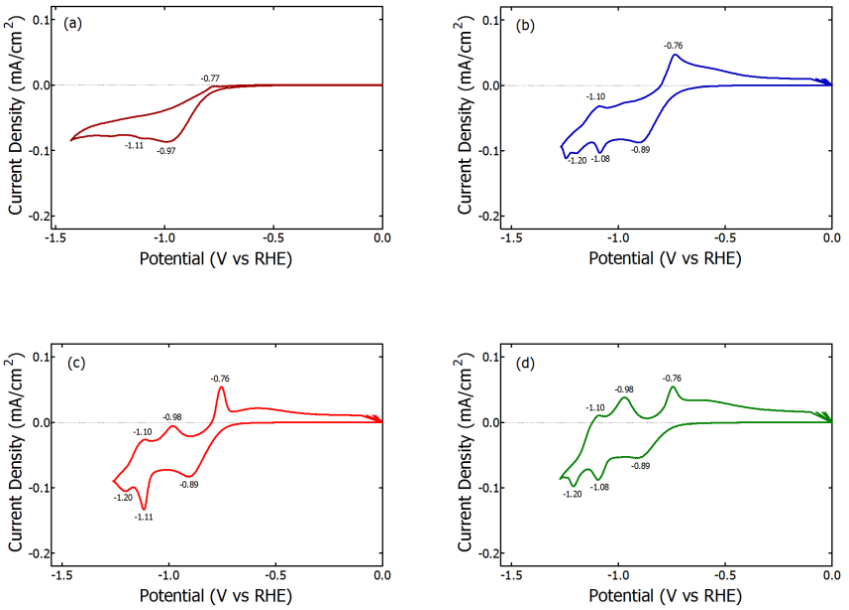

FIGURE 3.23
Cyclic voltammograms of Fe_2O_3 films coated on FTO under UV-Vis light illumination, which were heat-treated at various temperatures for 10 min in air. (a) Fe_2O_3 (= 27.16 wt%)/FTO at 500°C, (b) Fe_2O_3 (treated by TBAOH)/FTO at 420°C, (c) Fe_2O_3 (treated by TBAOH)/FTO at 500°C, and (d) Fe_2O_3 (treated by TBAOH)/FTO at 700°C

Oxidation-reduction reactions for the samples of fig 3.17 were observed by using cyclic voltammetry (CV) to investigate the effect of the surfactant and heat-treatment condition on the photo anode performance. CV data for samples heat-treated at 500°C with and without TBAOH treatment are shown in Figs.3.23 (a) and (c), respectively. The surfactant treated sample showed more reactions with higher current densities, which was consistent with the I-V data in Fig.3.16 (B) (surfactant treated). The sample heat-treated at 500°C (Fig.3.23 (c)) showed improved CV data compared to one heat-treated at 420°C (Fig.3.23 (b)). However, the performance was deteriorated when heat-treated at 700°C (Fig.3.23 (d)). These results were also consistent with the microstructure changes of the samples (Fig.3.16 (A)), where 700°C of heat-treatment caused particles' growth and agglomeration, contributing to more recombination of hole-electron pairs [24].

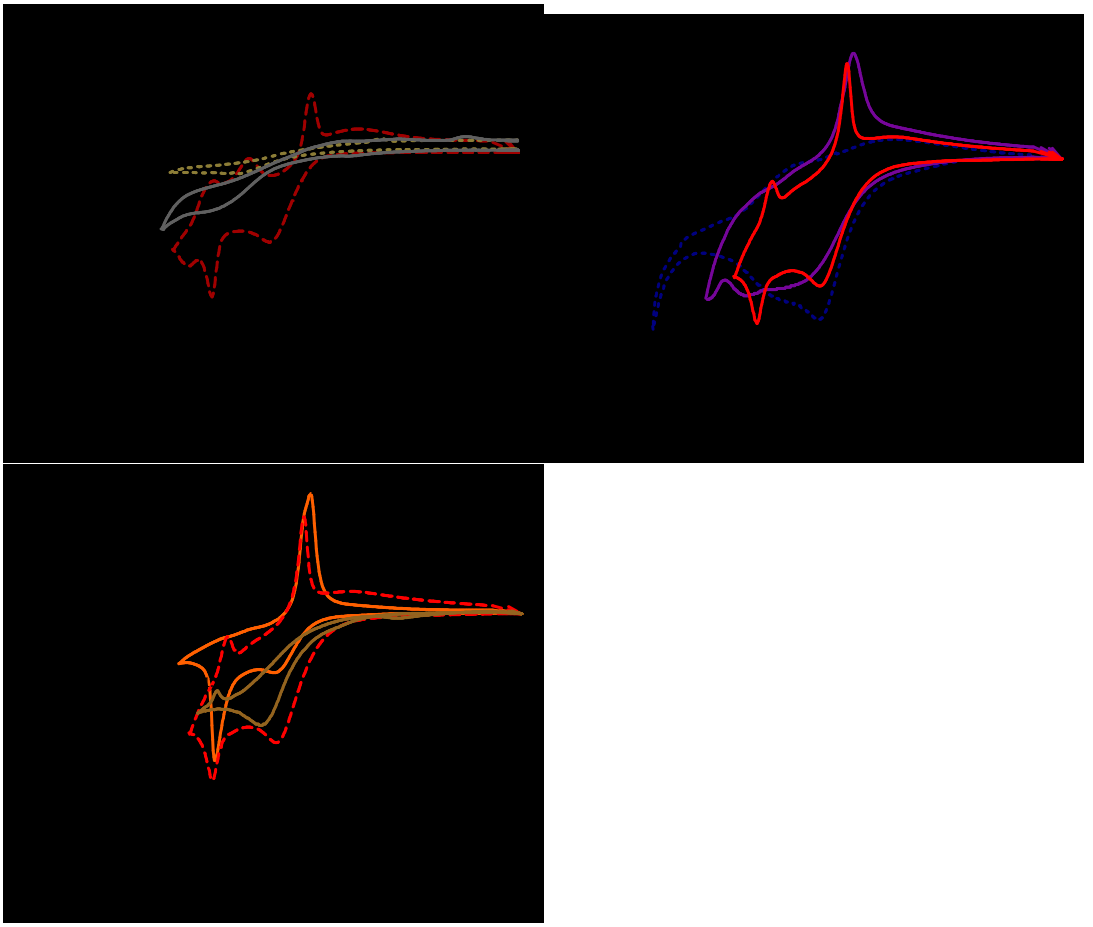

FIGURE 3.24
CV characteristics measured under 100 mW/cm^2 UV-Vis illumination: (A); (a) FTO glass, (b) TiO_2/FTO, and (c) Fe_2O_3/FTO samples were investigated after heat-treatment at 500^{o}C for 10 min in the air,(B); Fe_2O_3/TiO_2/FTO samples were became heat treated for 10 min in the air at (a) 420^{o}C, (b) 500^{o}C, and (c) 550^{o}C, (C); (a) Fe_2O_3/TiO_2/FTO and (b) TiO_2/Fe_2O_3/FTO heat treated at 500^{o}C for 10 min in the air, and (c) Fe_2O_3/TiO_2/FTO sample double heat treated, corresponding to (d) in Figure 3.19

On the other parts of our studying Oxidation-reduction redactions for the selected photo anode samples were observed by using cyclic voltammetry (CV) to investigate the effect of the coating sequence of constituent films and heat-treatment condition on the photo electrode performance. CV data for the samples of FTO glass, TiO_2/FTO, and Fe_2O_3/FTO were obtained as a reference in figure 3.24(A)-(a), (b) and (c), respectively. As expected the sample including Fe_2O_3 showed active reactions with the applied potential. According to the data (figure 3.24(B)) from the Fe_2O_3/TiO_2/FTO samples heat treated at the various temperatures of 420 ~ 550^{o}C for 10 min, the samples heat treated at 500^{o}C showed multiple oxidation-reduction peaks, contributing to higher photocurrent density. These results were found to be consistent with I-V data of the samples described in figure 3.18 where the sample heat-treated at 500^{o}C showed best performance. The sample of Fe_2O_3/TiO_2/FTO which showed best result after heat treatment at 500^{o}C was then compared with TiO_2/Fe_2O_3/FTO sample to see the effect of the location of TiO_2 layer placed in the photo anode, which was also heat treated under the same

condition. These samples showed a clear contrast in the results as shown in figures 3.24 (C)-(a) and (b), respectively: Fe_2O_3/TiO_2/FTO sample produced more and clear oxidation-reduction peaks. On the other hand, the sample of Fe_2O_3/TiO_2/FTO, which was heat-treated twice after each coating of TiO_2 and Fe_2O_3 layers, showed an intermediate performance (figure 3.24 (C)-(c)). All these results were along with the I-V data in figure 3.19 where the sample of Fe_2O_3/TiO_2/FTO heat-treated once (figure 3.19(b)) at 500°C, so it showed best performance followed by the sample double heat treated (figure 3.19(d)), and TiO_2/Fe_2O_3/FTO sample (figure 3.19(c)) [12].

Conclusion

In our study H-TiNT particles were coated porously on an FTO glass using the LBL-SA method and then heat-treated at temperatures below 600°C for 10 min in air for proper water splitting electrodes. Among the samples, the TiNT/TiO_2 film of mixed phases heat-treated at 500°C gained the maximum current value at applied voltages under UV-A irradiation, together with the appropriate porosity as well as the increased electrical conductivity by sintering. For the effective photo electrochemical performance of the Fe_2O_3 photoanode, the optimum amount of Fe_2O_3 particles was selected. At about 27 - 50 wt% Fe_2O_3, the best photocurrent density of about 0.96 mA/cm^2 was obtained at 1.23 (V vs. RHE), which was 5 times improvement when compared with the FTO sample without Fe_2O_3 photoanode. To improve the photoelectrochemical performance of the Fe_2O_3 photoanode under the optimum amount of Fe_2O_3 particles, the effect of microstructures was investigated, which were modified by a surfactant and heat-treatment. The Fe_2O_3 particles, obtained from Fe $(NO_3)_3$ treated with TBAOH surfactant were observed to be well dispersed while being coated on the FTO substrate. The particles also maintained nano-scaled size without much agglomeration and thermally activated growth during the optimized heat-treatment condition at 500°C for 10 min with the heating rate of 500°C/sec, contributed to the improvement of the PEC performance. The photocurrent density of the sample, processed with TBAOH surfactant and optimum heat-treatment, was measured to be about 1.32 mA/cm^2 at 1.23 (V vs. RHE), which was about a 32 % improvement compared with the sample not surfactant treated. Thus, it can be concluded from the current results that modification of the microstructure by the application of a surfactant together with an optimized heat-treatment is a promising way to improve the electrochemical performance of the photoanode. As a way of improving the performance of the Fe_2O_3-based photo anode for a photo electrochemical water-splitting system, a photo catalytic layer of TiO_2 film was structured into Fe_2O_3/FTO photo anode as an interlayer. The role of the photo catalytic interlayer conceived in this study was to modify energy bands and facilitate electron transfer to the electron collector in the photo anode; these were confirmed from the related UV-Vis absorbance and CV data. The photo electrochemical performance with the TiO_2 interlayer showed a significant improvement in the photocurrent density as well as the onset voltage for photocurrent generation. Our results suggest that preparing a photo anode with a photo catalytic interlayer of TiO_2 is a promising approach to generating photocurrent closer to the theoretical amount at a reduced onset voltage. Morphology and crystallite structures in relation to the performance of the photo electrode of Fe_2O_3/ H-TiNT/ FTO film were investigated with the annealing temperatures of 420-550°C. The phase of TiO_2 interlayer plays a critical role in improving the photo electrode performance. The best result was obtained with the photo electrode when heat-treated to possess double phase of H-TiNT and anatase-TiO_2 in the electrode. On the other hand, the microstructure changes of Fe_2O_3 by annealing did not seem to make much effect on the performance improvement. In conclusion, our study suggests that photo electrode with mixed phases of H-TiNT and anatase-TiO_2 in the TiO_2 interlayer by appropriate heat treatment can be a promising candidate to improve the performance for

efficient water splitting. Fe_2O_3-TiO_2 based photo anodes for water splitting were synthesized on the FTO substrate and their performance results were understood from the microstructure and energy band aspects. Comparatively, the photoanode (Fe_2O_3/TiO_2/FTO) comprising top layer of α-Fe_2O_3 nanoparticles along with the interlayer having mixed phases of H-TiNT/ anatase-TiO_2 showed best performance. The nano-scaled Fe_2O_3 particles with high uniformity were observed to contribute to the performance enhancement. In addition, the presence of the Fe_2O_3 nanoparticles in the middle and bottom layers caused by the infiltration of the precursor solution of Fe_2O_3 during synthesis seemed to modify the energy band structure to more favorable one for efficient electrons transfer. Our current results suggest that the application of the TiO_2 interlayer, together with optimized amount of α- Fe_2O_3 nanoparticles present in the constituent layers, could significantly contribute to the performance improvement of the conventional Fe_2O_3 photo anode.

Acknowledgments

This research was supported by the National Research Foundation of Korea Grant foundation by the Korean Government (NRF-2011-0016699).

References

1. Murphy AB, Barnes PRF, Randeniya LK, Plumb IC, Grey IE, Horne MD, Glasscock JA. Efficiency of solar water splitting using semiconductor electrodes. International journal of hydrogen energy 2006; 31, 1999.
2. Watanabe A, Kozuka H. Photoanodic Properties of Sol-Gel-Derived Fe2O3 Thin Films Containing Dispersed Gold and Silver Particles. J. Phys. Chem. B 2003; 107, 12713.
3. Bendavid A, Martin P. J, Jamting A, Takikawa H. Structural and optical properties of titanium oxide thin films deposited by filtered arc deposition. Thin Solid Films 1999; 356, 6-11.
4. Santato C, Ulmann M, Augustynski J. Enhanced Visible Light Conversion Efficiency Using Nanocrystalline WO_3 Films. Advanced Materials 2001; 13, 511- 514.
5. Zhu J, Ren J, Huo Y, Bian Z and Li H. Nanocrystalline Fe/TiO_2 Visible Photocatalyst with a Mesoporous Structure Prepared via a Nonhydrolytic Sol–Gel Route. Journal of Physical Chemistry 2007; 111, 18965-18969.
6. Xing M, Zhang J, Chen F. Photocatalytic Performance of N-Doped TiO_2 Adsorbed with Fe^{3+} Ions under Visible Light by a Redox Treatment. Journal of Physical Chemistry 2009; 113, 12848–12853.
7. Zhang H, Zhu H. Preparation of Fe-doped TiO_2 nanoparticles immobilized on polyamide fabric. Applied Surface Science 2012; Vol.258(24), 10034-10041.
8. Cam Loc L, Quoc Tuan N and Si Thoang H. Synthesis and characterization of Fe-doped TiO_2 photocatalyst by the sol–gel method. Nanoscience and Nanotechnology 2010; 015008 (5pp).
9. Oh H. J, Noh K. J, Kim B. R, Kang W. S, Jung S. C and Kim S. J. Fabrication of Fe_2O_3/TiO_2 Photoanode for Improved Photoelectrochemical Water Splitting. Japanese Journal of Applied Physics 2013; 52 01AC15.

10. Noh K-J, Oh H-J, Ku H-K, Kung S-C, Kang W, Park S and Kim S-J. Annealing Effect on the Microstructure and Electrochemical Properties of Fe_2O_3/H-TiNT/FTO Thin Film. Journal of Nanoscience and Technology 2013; 13, 1863-1866.
11. Noh K-J, Oh H.-J, Kim B-R, Jung S-C, Kang W and Kim S-J. Photoelectrochemical Properties of Fe_2O_3 Supported on TiO_2-Based Thin Films Converted from Self-Assembled Hydrogen Titanate Nanotube Powders. Journal of Nanomaterials 2012; 475430-475436.
12. Noh E, Noh K. J, Yun K. S, Kim B. R, Jeonh H. J, Oh H. J, Jung S. C, Kang W. S and Kim S. J. Enhanced Water Splitting by Fe_2O_3-TiO_2-FTO Photoanode with Modified Energy Band Structure. The Scientific World Journal 2013; 723201-723209.
13. Qamar M, Yoon C-R, Oh H.-J, Lee N-H, Park K, Kim D-H, Lee K-S, Lee W-J, and Kim S-J. Preparation and photocatalytic activity of nanotubes obtained from titanium dioxide. Science Direct 2008; 3-14.
14. Oh H-J, Noh K-J, Ku H-K, Park K-S, Jung S-C, Lee W-J, and Kim S-J. Preparation of Hydrogen Titanate Nanotube/FTO Glass Thin Film Obtained by the Layer-by-Layer-Self Assembling Method for Water Splitting. Journal of Nanoscience and Nanotechnology 2011; 7210-7213.
15. Oh H-J, Noh K-J, Ku H-K, Jung S-C, Lee W-J, Kang W-S and Kim S-J. Preparation of various metal ions doped hydrogen titanate nano particle coated thin films by layer-by-layer self-assembling method for an electrochromic electrode. Progress in Organic Coatings 2012; 745-749.
16. Wang Y, Yu T, Chen X, Zhang H, Ouyang S, Li Z, Ye J, Zou Z. Enhancement of Photoelectric Conversion Properties of $SrTiO_3$/α-Fe_2O_3 Heterojunction Photoanode. Journal of Physics D Applied Physics 2007; 40, 3925-3930.
17. Palmas S, Polcaro A. M, Ruiz J. R, Pozzo A. D, Mascia M and Vacca A. TiO_2 photoanodes for electrically enhanced water splitting. International Journal of Hydrogen Energy 2010; 6561–6570.
18. Tilley S. D, Cornuz M, Sivula K and Gratzel M. Light-InducedWater Splitting with Hematite: Improved Nanostructure and Iridium Oxide Catalysis. Angewandte Chem International Edition 2010; 49, 6405 –6408.
19. Hattori A, Tokihisa Y, Tada H, Tohge N, Ito S, Hongo K, Shiratsuchi R and Nogami G. Patterning Effect of a Sol-Gel TiO_2 Overlayer on the Photocatalytic Activity of a TiO_2/SnO_2 Bilayer-Type Photocatalyst. Journal of Sol-Gel Science and Technology 2001; 53–61.
20. Xu Z and Yu J. Visible-light-induced photoelectrochemical behaviors of Fe-modified TiO_2 nanotube arrays. Nanoscale 2011; 3138-3144.
21. Zhang J, Yu J, Zhang Y, Li Q and Gong J. R. Visible Light Photocatalytic H_2-Production Activity of CuS/ZnS Porous Nanosheets Based on Photoinduced Interfacial Charge Transfer. Nano Lett 201; 4774-4779.
22. Ingler Jr W. B and Khan S. U. Photoresponse of spray pyrolytically synthesized magnesium-doped iron (III) oxide (p-Fe_2O_3) thin films under solar simulated light illumination. Thin Solid Films2004; 301-308.
23. Hu Y. S, Kleiman-Schwarsctein A, Forman A. J, Hazen D, Park J. N and McFarland E. W. Pt-Doped α-Fe_2O_3 Thin Films Active for Photoelectrochemical Water Splitting. Chemistry of Materials 2008; 3803-3805.

24. Noh K. J, Kim B. R, Yoon G. J, Jung S. C, Kang W and Kim S. J. Microstructural Effect on the Photoelectrochemical Performance of Hematite-Fe_2O_3 Photoanode for Water Splitting. Electronic Materials Letters 2012; 345-350.